Stable high order space-time finite element formulation for large displacement elastodynamics

Darcy Hannah Falcão Rangel Moreira[1], Weslley Camargo Lopes[1], Rodolfo André Kuche Sanches[1]

[1]*Structural Engineering Department, São Carlos School of Engineering, University of São Paulo*
Av. Trabalhador Saocarlense, 400, São Carlos, São Paulo, Brazil
darcyhannah@usp.br, weslley.lopes@usp.br, rodolfo.sanches@usp.br

Abstract. Direct time integration methods have been widely used in structural and solid dynamics simulations, specially in nonlinear problems. Time-marching methods have been applied to discrete systems of differential equations obtained from different spatial discretization techniques, like finite differences, finite volume, boundary elements and finite elements, with finite elements being currently the most applied method for structural and solid mechanics. On the other hand, space-time formulations consider time as a dimension of the finite element discretization, so that the precision in time integration can be increased by using higher order shape functions in time direction. In this context, this work presents a position-based total Lagrangian space-time finite element formulation for the solution of two-dimensional elasticity problems with large displacements. By using structured space-time mesh in time direction, it is possible to divide the space-time domain into space-time slabs, so that such slabs can be solved progressively with the final nodal positions and velocities from previous slab being applied as initial conditions to the current one. The adopted space-finite elements are prismatic with a triangular basis corresponding to the spatial discretization and height corresponding to the temporal discretization, so that the space-time shape functions are given by the product of the Lagrange polynomial shape functions adopted for the triangular elements of spatial discretization, with Hermite polynomials based shape functions defined along the height of the prism, for time discretization. The test functions in time direction are modified so that different stability and precision can be achieved. Through the simulation of selected examples, and the comparison with solutions from known time-marching methods, the robustness and stability of the proposed formulation is demonstrated.

Keywords: space-time formulation, positional-based formulation, stable high order time integration, time-marching methods, large displacements

1 Introduction

Resonant systems, floating platforms, parachute systems, and blood valves are examples of structures or structural systems that experience significant displacements during operation. Over the years, various formulations of the finite element method (FEM) based on displacements have been developed to address these types of problems [1–7]. The corotational approach [8–14], which describes finite element movement through nodal displacements and rotations in a rotating frame of reference aligned with the element, has proven robust in addressing geometric nonlinearity. Alternatively, Coda, inspired by Bonet et al., introduced and systematized the positional-based formulation of FEM that consider the positions as unknowns, enabling balance equations to be defined in the deformed state and seamlessly incorporating geometric nonlinearity. Hence, the formulation has a great potential in scenarios involving large displacements, as can be seen in several works dealing with elastic material [17–28].

In dynamic problems, time-marching methods are often employed to solve the system of differential equations resulting from spatial discretization. A classic implicit time-marching technique is the average acceleration method - family member of Newmark's method [29]. Its numerical characteristics have been investigated for both linear [30] and nonlinear [31] regimes.

Conversely, the space-time formulation of FEM applies finite element techniques to both spatial and temporal domains. The fully discretized problem involves a space-time mesh composed of interconnected elements linked by nodes, each associated with space-time shape functions. Elements can be simplex, leading to an unstructured

mesh suitable for adaptive techniques, or prismatic—resulting from the Cartesian product of spatial and temporal finite elements—creating a structured mesh [32]. The structured space-time mesh approach shares similarities with time-marching methods [33], as problem solutions can be sequenced and information propagates along the positive time axis direction.

Within the framework of a structured space-time mesh, the Time FEM addresses temporal problems [34–41], starting from the spatially discretized system. The key challenge lies in selecting temporal shape functions to achieve stability and convergence throughout the solution. Notably, this approach permits stability analysis using one-degree-of-freedom systems. By using linear shape functions within a Discontinuous Galerkin framework, Hulbert and Li and Wiberg obtained unconditionally stable algorithms. Other works utilized cubic Hermite polynomials [35, 38, 41], introducing nodal velocities as degrees of freedom, yet offering the advantage of strongly accounting for initial conditions. Fung introduced shape functions based on cubic Hermite polynomials to achieve algorithms with unconditional stability and high convergence orders. One such algorithm attained fourth-order convergence and unconditional stability, proving suitable for solid mechanics applications, where lower vibration modes significantly influence most problems of interest.

A drawback of the space-time FEM is its greater computational cost compared to FEM with time-marching methods. However, high temporal convergence orders can be achieved using temporal shape functions, allowing for larger time steps with sufficient precision. In light of this, our work aims to present a space-time formulation of the finite element method. Constructed within a structured mesh framework employing a total Lagrangian description, this formulation utilizes position-based spatial discretization and implements the fourth-order unconditionally stable integrator suggested by Fung for temporal solutions. Our study will juxtapose these outcomes against those derived from Newmark's method in conjunction with position-based FEM, along with existing findings in the literature.

2 Space-time formulation

2.1 Problem statement

Let be the space-time domain $Q = \Omega \times [0, T]$, where $\Omega \subset \mathbb{R}^{n_d}$ is a closed boundary domain with boundary Γ, where $n_d \leq 3$ is the number of spatial dimensions and T the final time. The boundary is $\Gamma = \Gamma^D \cup \Gamma^N$, so that $\Gamma^D \cap \Gamma^N = \varnothing$, being Γ^D and Γ^N the Dirichlet and Neumann boundaries, respectively. On the other hand, the space-time boundary is given by $R = \Gamma \times [0, T]$, so that $R = R^D \cup R^N$, being $R^D \cap R^N = \varnothing$, with R^D and R^N called space-time Dirichlet and Neumann boundaries, respectively. Considering the total Lagrangian description, the initial configuration Ω_0, with boundary Γ_0 and points $\mathbf{x} \in \Omega_0$, is projected (extruded) along the time axis in order to obtain the reference domain $\bar{Q} = \Omega_0 \times [0, T]$ with boundary $\bar{R} = \Gamma_0 \times [0, T]$, which serves as an auxiliary domain for calculating the strains at each time. Given these considerations, the momentum balance equation is written as:

$$\nabla_{\mathbf{x}} \cdot \mathbf{P} + \mathbf{b}_0 = \rho_0 \ddot{\mathbf{y}} \quad \text{in} \quad \bar{Q}, \tag{1}$$

where $\mathbf{y} \in \Omega$ is the position of an observed particle at the current time, and therefore $\ddot{\mathbf{y}}$ is its acceleration, obtained from the material derivative of its velocity $\dot{\mathbf{y}} = \partial \mathbf{y}/\partial t$, $\rho_0(\mathbf{x})$ is the initial density, $\mathbf{b}_0$ is the vector of domain forces acting on the initial configuration, the $\nabla_{\mathbf{x}}(\bullet)$ symbol representing the gradient of $(\bullet)$ with respect to the initial coordinates $\mathbf{x}$, and $\mathbf{P} = \boldsymbol{\sigma}^T \cdot \mathbf{F}^{-T}$ is the first Piola-Kirchhoff stress tensor, being $\mathbf{F} = \partial \mathbf{y}/\partial \mathbf{x}$ the deformation gradient and $J = \det \mathbf{F}$.

A more appropriate stress tensor in mathematical developments is the second Piola-Kirchhoff stress tensor, given by $\mathbf{S} = \mathbf{F}^{-1} \cdot \mathbf{P}$. By assuming the isotropic linear elasticity, with small to moderate deformations, $\mathbf{S}$ is related to the Green-Lagrange deformation tensor $\mathbf{E} = \frac{1}{2}(\mathbf{F}^T\mathbf{F} - \mathbf{I})$, where $\mathbf{I}$ is the second-order identity tensor of dimension $n_d \times n_d$, through the constitutive law of Saint-Venant-Kirchhoff, given by: $\mathbf{S} = 2\mathbf{E} + \lambda \text{tr}(\mathbf{E})\mathbf{I}$, where $\mu = E/[2(1+\nu)]$ and $\lambda = \nu E/(1+\nu)/(1-2\nu)$ the Lammé constants.

The complete definition of the problem is achieved when considering the boundary and initial conditions, given by:

$$\mathbf{y}(\mathbf{x}, t) = \bar{\mathbf{y}}(\mathbf{x}, t) \quad \text{on} \quad \bar{R}^D \tag{2}$$

$$\mathbf{P} \cdot \mathbf{n}_0 = \mathbf{t}_0(\mathbf{x}, t) \quad \text{on} \quad \bar{R}^N \tag{3}$$

$$\mathbf{y}(\mathbf{x}, 0) = \mathbf{y}^0(\mathbf{x}) \quad \text{in} \quad \Omega_0 \tag{4}$$

$$\dot{\mathbf{y}}(\mathbf{x}, 0) = \mathbf{v}^0(\mathbf{x}) \quad \text{in} \quad \Omega_0, \tag{5}$$

where $\bar{\mathbf{y}}(\mathbf{x}, t)$ is the current positions prescribed in $\bar{R}^D$, $\mathbf{t}_0$ the vector of surface forces applied at $\bar{R}^N = \Gamma_0^N \times [0, T]$ with $\mathbf{n}_0$ being the outward normal vector to Γ_0^N, and $\mathbf{y}^0(\mathbf{x})$ and $\mathbf{v}^0$ the initial positions and velocities, respectively.

2.2 Space-time discretization

Let $\bar{Q}^h$ with boundary $\bar{R}^h$ be the approximate reference domain. This is divided into space-time slabs, defined as $\bar{Q}_n^h = \Omega_0^h \times I_n^h$ with boundary $\bar{R}^h = \Gamma_0^h \times I_n^h$. It can be established that $\bar{Q} \approx \bar{Q}^h = \bigcup_{n=0}^{N-1} \bar{Q}_n^h$, with $\bar{Q}_n^h = \bigcup_{e=1}^{n_{ne}} \bar{Q}^e$ and $\bar{R} \approx \bar{R}^h = \bigcup_{n=0}^{N-1} \bar{R}_n^b$, with $\bar{R}_n^h = \bigcup_{b=1}^{n_{eb}} \bar{R}^b$, where $\bar{Q}_n^e$ are the space-time elements. Assuming structured meshes, the reference space-time slab is the product of the spatial mesh of the solid in its initial configuration and the time step (height of the current slab). Therefore, it is noted that it is more convenient to represent a space-time finite element by means of the Cartesian product between a spatial element Ω_0^e and a temporal element $I_n = [t_n, t_{n+1}]$, where t_n and t_{n+1} is the initial and current time (or nodes) of a temporal element of size $\Delta t = t_{n+1} - t_n$, so that $\bar{Q}_n^e = \Omega_0^e \times I_n$.

Position-based spatial discretization

In the context of spatial elements Ω_0^e, each node a is associated with a Lagrangian shape function $\phi_a(\boldsymbol{\xi})$. Here, $\boldsymbol{\xi}$ represents a dimensionless coordinate system unique to each finite element. These shape functions serve as the foundation for expressing both the initial configuration Ω_0^e and the current configuration Ω^e in the following manner:

$$\mathbf{x}^h(\boldsymbol{\xi}) = \mathbf{f}^0(\boldsymbol{\xi}) = \phi_a(\boldsymbol{\xi})\mathbf{x}_a, \tag{6}$$

$$\mathbf{y}^h(\boldsymbol{\xi}, t) = \mathbf{f}^1(\boldsymbol{\xi}, t) = \phi_a(\boldsymbol{\xi})\mathbf{y}_a(t). \tag{7}$$

In these equations, $\mathbf{x}_a$ and $\mathbf{y}_a$ correspond to vectors with dimensions $n_d \leq 3$, containing the initial and current coordinates of the node a, respectively. Through the composition of mappings $\mathbf{f}^0$ and $\mathbf{f}^1$, the overall deformation function of the element can be expressed as $\mathbf{f}^h(\mathbf{x}, t) = \mathbf{f}^1(\boldsymbol{\xi}, t) \circ (\mathbf{f}^0(\boldsymbol{\xi}))^{-1}$. This leads to the element's deformation gradient $\mathbf{F}^h = \mathbf{F}^1 \cdot (\mathbf{F}^0)^{-1}$, where $\mathbf{F}^0 = \partial \mathbf{f}^0 / \partial \boldsymbol{\xi}$ and $\mathbf{F}^1 = \partial \mathbf{f}^1 / \partial \boldsymbol{\xi}$ denote the gradients of the initial and current mappings respectively.

Temporal discretization based on Hermite cubic polynomials

Similarly, a temporal finite element consists of two nodes, each featuring two degrees of freedom - position and velocity. Corresponding to each degree of freedom b, there is an associated temporal shape function denoted as ψ_b. Consequently, the temporal finite element is composed of four shape functions, based on Hermite cubic polynomials, which are as follows:

$$\psi_1(\theta) = \frac{1}{4}(1-\theta)^2(2+\theta), \tag{8}$$

$$\psi_2(\theta) = \frac{\Delta t}{8}(1+\theta)(1-\theta)^2, \tag{9}$$

$$\psi_3(\theta) = \frac{1}{4}(1+\theta)^2(2-\theta), \tag{10}$$

$$\psi_4(\theta) = -\frac{\Delta t}{8}(1+\theta)^2(1-\theta), \tag{11}$$

where $\theta \in [-1, 1]$ is the dimensionless local coordinate. Considering that time is interpolated by $t = (\theta+1)\Delta t/2 + t_n$, the behavior of the position degree of freedom of a node a ($\mathbf{y}_a(t)$ in the equation(7)) in the interior of a finite temporal element is interpolated as:

$$\mathbf{y}_a(\theta) = \psi_1(\theta)\mathbf{y}_a^n + \psi_2(\theta)\mathbf{v}_a^n + \psi_3(\theta)\mathbf{y}_a^{n+1} + \psi_4(\theta)\mathbf{v}_a^{n+1}, \tag{12}$$

from where it is important to note that $\mathbf{y}_a^{n+1}$ and $\mathbf{v}_a^{n+1}$ signify the unknowns in the given problem.

2.3 Numerical solution via weighted residual method

Regarding the n-th reference slab $\bar{Q}_n^h$, we establish finite-dimensional spaces: $\mathcal{Y}^h$ for the trial function $\mathbf{y}^h(\mathbf{x}, t)$ and $\mathcal{W}^h$ for test functions $\mathbf{w}^h(\mathbf{x}, t)$. These spaces comprise suitably differentiable functions to effectively approximate the mentioned functions. In $\mathcal{Y}^h$, functions satisfy $\mathbf{y}^h = \bar{\mathbf{y}}$ over $(\bar{R}_n^D)^h$, while in $\mathcal{W}^h$, functions and their derivatives are homogenous at t_n, i.e., $\mathbf{w}^h(\mathbf{x}, t_n) = \mathbf{0}$ and $\dot{\mathbf{w}}^h(\mathbf{x}, t_n) = \mathbf{0}$.

The test function is defined as:

$$\mathbf{w}^h(\boldsymbol{\xi}, \theta) = \phi_a(\boldsymbol{\xi})\mathbf{w}_a(\theta), \tag{13}$$

where

$$\mathbf{w}_a(\theta) = \psi_1^w(\theta)(\mathbf{w}_a)_1^n + \psi_2^w(\theta)(\mathbf{w}_a)_2^n + \psi_3^w(\theta)(\mathbf{w}_a)_3^{n+1} + \psi_4^w(\theta)(\mathbf{w}_a)_4^{n+1}, \tag{14}$$

and ψ_b^w, with $b = 1, 2, 3, 4$, the shape functions of the test function.

By employing the weighted residuals method, the discrete initial-boundary value problem can be expressed as follows: finding $\mathbf{y}^h \in \mathcal{Y}^h$, so that $\forall\ \mathbf{w}^h \in \mathcal{W}^h$:

$$\int_{\bar{Q}_n} (\rho_0 \ddot{\mathbf{y}}^h - \nabla_{\mathbf{x}} \cdot \mathbf{P}^h - \mathbf{b}_0^h) \cdot \mathbf{w}^h \, d\bar{Q}_n = \int_{t_n}^{t_{n+1}} \int_{\Omega_0} (\rho_0 \ddot{\mathbf{y}}^h - \nabla_{\mathbf{x}} \cdot (\mathbf{F}^h \cdot \mathbf{S}^h) - \mathbf{b}_0^h) \cdot \mathbf{w}^h \, d\Omega_0 \, dt = 0, \tag{15}$$

In this equation, it's evident that the domain of integration in the first integral is localized within a reference space-time slab, while in the second integral, the independence of spatial and temporal integrations is evident. This formulation exhibits resemblance to time-marching methods. Notably, it can handle distinct and independent discretizations (structured meshes) for space and time. The solution is achieved sequentially, where the final conditions of a slab become the initial conditions of the subsequent one.

Expanding equation (15) and eliminating a set of nodal parameters from the test function yields a determinate system of equations (two equations and two unknowns). Interestingly, by adopting $\psi_b^w = \psi_b$ (i.e., using the same temporal shape functions for both test and trial functions), six conditionally stable integrators similar to those derived by Mergel et al. emerge. Among them, a fourth-order convergent integrator named $p2$ stands out. On the other hand, Fung introduce two shape functions that can be incorporated into the 2x2 system of equations, leading to an unconditionally stable fourth-order time integrator. By discarding $(\mathbf{w}_a)_1^n$ and $(\mathbf{w}_a)_2^n$, and simplifying while retaining the arbitrariness of the remaining two parameters, (15) can be expressed as:

$$\int_{t_n}^{t_{n+1}} (\mathbf{f}_a^{inerc} + \mathbf{f}_a^{int} + \mathbf{f}_a^{ext}) \begin{Bmatrix} \psi_3^w \\ \psi_4^w \end{Bmatrix} dt \quad = \quad \mathbf{0}, \tag{16}$$

where:

$$\mathbf{f}_a^{iner} = \int_{\Omega_0^h} m_{ab} \ddot{\mathbf{y}}_b \, d\Omega_0^h, \tag{17}$$

$$\mathbf{f}_a^{int} = \int_{\Omega_0^h} \mathbf{F}^h \cdot \mathbf{S}^h \cdot \frac{\partial \phi_a}{\partial \mathbf{x}} \, d\Omega_0^h, \tag{18}$$

$$\mathbf{f}_a^{ext} = -\int_{\Gamma_0^{N\,h}} \phi_a \mathbf{t}_0^h \, d\Gamma_0^{N\,h} - \int_{\Omega_0^h} \phi_a \mathbf{b}_0^h \, d\Omega_0^h, \tag{19}$$

are the inertial, internal and external nodal forces, respectively, and $m_{ab} = \int_{\Omega_0^h} \rho_0 \phi_a \phi_b \, d\Omega_0^h$ a scalar quantity of mass. The shape functions ψ_3^w and ψ_4^w of the equation (16), taken from work of Fung, are given by:

$$\psi_3^w(\theta) = -140\bar{\theta}^3 + 210\bar{\theta}^2 - 90\bar{\theta} + 11, \tag{20}$$

$$\psi_4^w(\theta) = 280\bar{\theta}^3 - 420\bar{\theta}^2 + 180\bar{\theta} - 20, \tag{21}$$

where $\bar{\theta} = (\theta + 1)/2$.

3 Numerical examples

The subsequent numerical examples were simulated using Lagrange triangular elements. To solve the system of equations (16), the Newton-Raphson method was employed, with a predefined tolerance of 10^{-6}. Spatial integration was executed using Hammer quadrature points, while numerical integration in the temporal domain was carried out using Gaussian quadrature points

3.1 Bar under axial vibration

To validate the proposed formulation, we examined a simple wave problem involving a bar. The bar has dimensions of length 1.0 and height 0.05, subjected to a plane stress state with unit width. The left end is fixed, and a sudden axial load of intensity 1.0 per unit length is applied along the right vertical face. We used dimensionless quantities. The material is characterized by an elastic modulus of $\mathbb{E} = 1.0 \times 10^4$, Poisson's ratio $\nu = 0.0$, and

initial density $\rho_0 = 1.0$. The bar starts from rest, implying initial positions and velocities of zero. The analytical solution (see [43]) predicts a maximum amplitude of twice the static response ($u_1^{st} = 1.0 \times 10^{-4}$), resulting in $u_1^{max} = 2.0 \times 10^{-4}$, and a natural period of $T_n = 0.04$.

Numerical simulations were conducted using both the proposed space-time formulation and Newmark's method with optimal parameters. The spatial mesh comprised 40 quadratic elements, and two different time steps were used: $\Delta t = 10^{-4}$ and $\Delta t = 10^{-3}$. Figure 1 illustrates the solutions for the horizontal displacement at the right end of the bar. The results indicate that the numerical solution for $\Delta t = 10^{-4}$ is in close agreement with the analytical solution. However, for a larger time step ($\Delta t = 10^{-3}$), damping occurs in the solution over time, more pronounced in Newmark's method. This observation underscores the superior temporal precision of the proposed space-time formulation compared to Newmark's method.

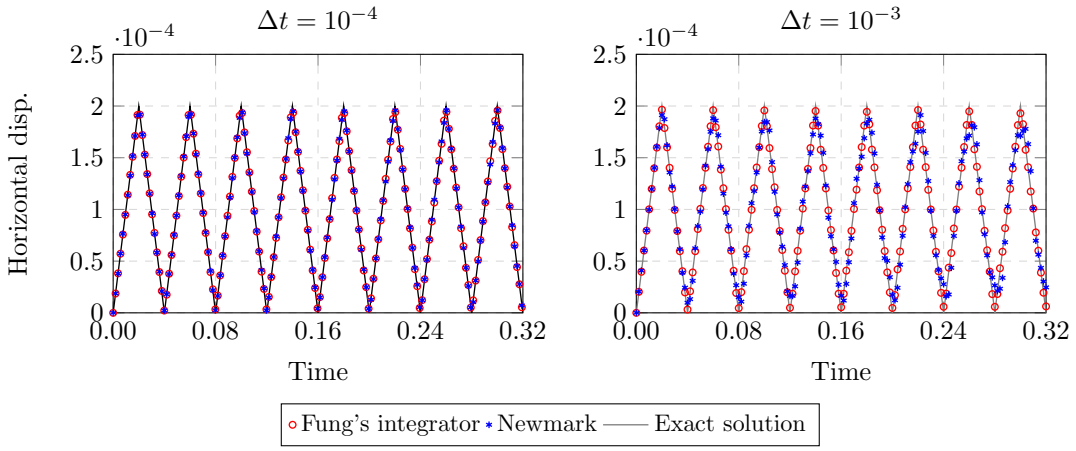

Figure 1. Horizontal displacement at the free end of the bar using two different time steps.

3.2 Cantilever beam under uniformly distributed load

We proceed to analyze a cantilevered beam subjected to a suddenly applied, uniformly distributed load of 2.85 lb/in along its length. The study aims to compare our results with those by Bathe et al.. The beam, featuring large displacements, is treated under a plane stress state with unit width. The elastic material adheres to the Saint-Venant-Kirchhoff law, with modulus of elasticity $\mathbb{E} = 1.2 \times 10^4$ lb/in², Poisson's ratio $\nu = 0.2$, and initial density $\rho_0 = 10^{-6}$ lb·s²/in^4. The beam dimensions are 10 in length and 1 in height. In the simulations by Bathe et al., five quadrangular elements with 8 nodes were used, employing Newmark's method with $\beta = 1/4$, $\gamma = 1/2$, and $\Delta t = 4.5 \times 10^{-5}$ s.

In our analysis, we employed a spatial mesh of 146 quadratic elements, adopting time steps of $\Delta t = 4.5 \times 10^{-5}$ s (matching the reference) and $\Delta t = 4.5 \times 10^{-4}$ s (10 times larger). Figure 2 presents the numerical results, showcasing the transversal displacement at the free end of the cantilever beam using the space-time formulation and Newmark's method with optimal parameters, alongside the outcomes of Bathe et al.. A good agreement is observed among all responses during the first oscillation period. For the second period, the space-time formulation with $\Delta t = 4.5 \times 10^{-4}$ exhibits a slight amplification in the response, while Newmark's method introduces an elongation in the oscillation period. From this, the space-time formulation presents superior accuracy than Newmark's method. Additionally, our solution is slightly flexible than Bathe et al.'s, possibly due to the difference in the number of elements used.

4 Conclusion

In this work, we introduced a position-based total Lagrangian space-time finite element formulation to tackle two-dimensional elasticity problems featuring large displacements. The formulation demonstrates its suitability for problems with large displacements, leveraging the inherent non-linearity of position-based FEM. Furthermore, we observed the higher numerical accuracy of the Fung formulation compared to Newmark's method, with the former being fourth-order and the latter second-order. The presented method proved stable and highly accurate even with larger time steps. In future research, we recommend exploring the computational performance of the proposed formulation against time-marching methods.

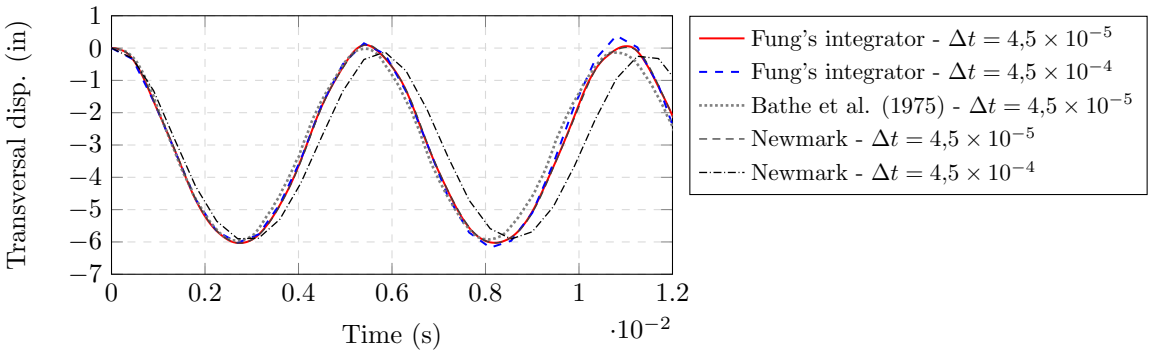

Figure 2. Transversal displacement at the free end of the cantilever beam using two different time steps.

Acknowledgements. This study was financed in part by the *Coordenação de Aperfeiçoamento de Pessoal de Nível Superior – Brasil* (CAPES), the *Brazilian Agency National Council for Scientific and Technological Development* (CNPq), and the *São Paulo Research Foundation* (FAPESP) – Process Number 2023/01688-8. The authors would like to thank them for the financial support given to this research.

Authorship statement. The authors hereby confirm that they are the sole liable persons responsible for the authorship of this work, and that all material that has been herein included as part of the present paper is either the property (and authorship) of the authors, or has the permission of the owners to be included here.

References

[1] J. Oden and T. Sato. Finite strains and displacements of elastic membranes by the finite element method. *International Journal of Solids and Structures*, vol. 3, n. 4, pp. 471–488, 1967.
[2] H. Hibbitt, P. Marcal, and J. Rice. A finite element formulation for problems of large strain and large displacement. *International Journal of Solids and Structures*, vol. 6, n. 8, pp. 1069–1086, 1970.
[3] J. C. Simo, K. D. Hjelmstad, and R. L. Taylor. Numerical formulations of elasto-viscoplastic response of beams accounting for the effect of shear. *Computer Methods in Applied Mechanics and Engineering*, vol. 42, n. 3, pp. 301–330, 1984.
[4] K.-J. Bathe, E. Ramm, and E. L. Wilson. Finite element formulations for large deformation dynamic analysis. *International Journal for Numerical Methods in Engineering*, vol. 9, n. 2, pp. 353–386, 1975.
[5] T. Belytschko, L. Schwer, and M. J. Klein. Large displacement, transient analysis of space frames. *International Journal for Numerical Methods in Engineering*, vol. 11, n. 1, pp. 65–84, 1977.
[6] M. A. Crisfield. *Nonlinear finite element analysis of solids and structures. Volume 1: Essentials*, 1991.
[7] J. Argyris, M. Papadrakakis, and Z. S. Mouroutis. Nonlinear dynamic analysis of shells with the triangular element tric. *Computer Methods in Applied Mechanics and Engineering*, vol. 192, n. 26, pp. 3005–3038, 2003.
[8] G. Wempner. Finite elements, finite rotations and small strains of flexible shells. *International Journal of Solids and Structures*, vol. 5, n. 2, pp. 117–153, 1969.
[9] T. Belytschko and B. J. Hsieh. Non-linear transient finite element analysis with convected co-ordinates. *International Journal for Numerical Methods in Engineering*, vol. 7, n. 3, pp. 255–271, 1973.
[10] C. Oran and A. Kassimali. Large deformations of framed structures under static and dynamic loads. *Computers & Structures*, vol. 6, n. 6, pp. 539–547, 1976.
[11] T. Belytschko and L. W. Glaum. Applications of higher order corotational stretch theories to nonlinear finite element analysis. *Computers & Structures*, vol. 10, n. 1, pp. 175–182, 1979.
[12] M. Crisfield. A consistent co-rotational formulation for non-linear, three-dimensional, beam-elements. *Computer Methods in Applied Mechanics and Engineering*, vol. 81, n. 2, pp. 131–150, 1990.
[13] B. Nour-Omid and C. Rankin. Finite rotation analysis and consistent linearization using projectors. *Computer Methods in Applied Mechanics and Engineering*, vol. 93, n. 3, pp. 353–384, 1991.
[14] M. Crisfield and G. Moita. A unified co-rotational framework for solids, shells and beams. *International Journal of Solids and Structures*, vol. 33, n. 20, pp. 2969–2992, 1996.
[15] H. B. Coda. An exact fem geometric non-linear analysis of frames based on position description. In *International Congress of Mechanical Engineering*. ABCM, 2003.
[16] J. Bonet, R. Wood, J. Mahaney, and P. Heywood. Finite element analysis of air supported membrane struc-

tures. *Computer Methods in Applied Mechanics and Engineering*, vol. 190, n. 5, pp. 579–595, 2000.
[17] M. Greco, F. Gesualdo, W. Venturini, and H. Coda. Nonlinear positional formulation for space truss analysis. *Finite Elements in Analysis and Design*, vol. 42, n. 12, pp. 1079–1086, 2006.
[18] H. Coda and M. Greco. A simple fem formulation for large deflection 2d frame analysis based on position description. *Computer Methods in Applied Mechanics and Engineering*, vol. 193, n. 33, pp. 3541 – 3557, 2004.
[19] H. B. Coda. A solid-like fem for geometrically non-linear 3d frames. *Computer Methods in Applied Mechanics and Engineering*, vol. 198, n. 47, pp. 3712–3722, 2009.
[20] H. B. Coda and R. R. Paccola. A fem procedure based on positions and unconstrained vectors applied to non-linear dynamic of 3d frames. *Finite Elements in Analysis and Design*, vol. 47, n. 4, pp. 319–333, 2011.
[21] H. B. Coda and R. R. Paccola. An alternative positional fem formulation for geometrically non-linear analysis of shells: Curved triangular isoparametric elements. *Computational Mechanics*, vol. 40, n. 1, pp. 185–200, 2007.
[22] H. B. Coda and R. R. Paccola. A positional fem formulation for geometrical non-linear analysis of shells. *Latin American Journal of Solids and Structures*, vol. 5, n. 3, pp. 205 – 223, 2008.
[23] H. Coda and R. Paccola. Unconstrained finite element for geometrical nonlinear dynamics of shells. *Mathematical Problems in Engineering*, vol. 2009, 2009.
[24] R. A. K. Sanches and H. B. Coda. Unconstrained vector nonlinear dynamic shell formulation applied to fluid-structure interaction. *Computer Methods in Applied Mechanics and Engeneering*, vol. 259, pp. 177–196, 2013.
[25] M. Sampaio, R. Paccola, and H. Coda. A geometrically nonlinear fem formulation for the analysis of fiber reinforced laminated plates and shells. *Composite Structures*, vol. 119, pp. 799–814, 2015.
[26] J. P. Pascon and H. B. Coda. Large deformation analysis of functionally graded elastoplastic materials via solid tetrahedral finite elements. *Computers & Structures*, vol. 146, pp. 59–75, 2015.
[27] J. W. D. Fernandes, H. B. Coda, and R. A. K. Sanches. Ale incompressible fluid–shell coupling based on a higher-order auxiliary mesh and positional shell finite element. *Computational Mechanics*, vol. 63, n. 3, pp. 555–569, 2019.
[28] G. Avancini and R. A. Sanches. A total lagrangian position-based finite element formulation for free-surface incompressible flows. *Finite Elements in Analysis and Design*, vol. 169, pp. 103348, 2020.
[29] N. M. Newmark. A method of computation for structural dynamics. *Journal of the Engineering Mechanics Division*, vol. 85, n. 3, pp. 67–94, 1959.
[30] K. J. Bathe and E. L. Wilson. Stability and accuracy analysis of direct integration methods. *Earthquake Engineering & Structural Dynamics*, vol. 1, n. 3, pp. 283–291, 1972.
[31] T. J. Hughes. Stability, convergence and growth and decay of energy of the average acceleration method in nonlinear structural dynamics. *Computers & Structures*, vol. 6, n. 4, pp. 313–324, 1976.
[32] T. Hughes and G. Hulbert. Space-time finite element methods for elastodynamics: Formulations and error estimates. *Computer Methods in Applied Mechanics and Engineering*, vol. 66, pp. 339–363, 1988.
[33] C. Bajer and A. Podhorecki. Space-time element method in structural dynamics. *Archives of Mechanics*, vol. 41, 1989.
[34] M. Baruch and R. Riff. Hamilton's principle, hamilton's law - 6 to the n power correct formulations. *AIAA Journal*, vol. 20, n. 5, pp. 687–692, 1982.
[35] R. Riff and M. Baruch. Time finite element discretization of hamilton's law of varying action. *AIAA Journal*, vol. 22, n. 9, pp. 1310–1318, 1984.
[36] G. M. Hulbert. Time finite element methods for structural dynamics. *International Journal for Numerical Methods in Engineering*, vol. 33, n. 2, pp. 307–331, 1992.
[37] X. D. Li and N.-E. Wiberg. Structural dynamic analysis by a time-discontinuous galerkin finite element method. *International Journal for Numerical Methods in Engineering*, vol. 39, n. 12, pp. 2131–2152, 1996.
[38] T. C. Fung. Unconditionally stable higher-order accurate hermitian time finite elements. *International Journal for Numerical Methods in Engineering*, vol. 39, n. 20, pp. 3475–3495, 1996.
[39] M. Mancuso and F. Ubertini. An efficient time discontinuous galerkin procedure for non-linear structural dynamics. *Computer Methods in Applied Mechanics and Engineering*, vol. 195, n. 44, pp. 6391–6406, 2006.
[40] A. Idesman. A new high-order accurate continuous galerkin method for linear elastodynamics problems. *Computational Mechanics*, vol. 40, pp. 261–279, 2007.
[41] L. Wang and H. Zhong. A time finite element method for structural dynamics. *Applied Mathematical Modelling*, vol. 41, pp. 445–461, 2017.
[42] J. C. Mergel, R. A. Sauer, and S. Ober-Blöbaum. C1-continuous space-time discretization based on hamilton's law of varying action. vol. 1, 2015.
[43] H. B. Coda. *O método dos elementos finitos posicional: sólidos e estruturas - não linearidade geométrica e dinâmica*. EESC-USP, 2018.